Modeling and Control of a Dual Active Bridge for Energy Storage in DC Microgrid Applications

Frederico L. F. Marcelino, Hans H. Sathler
Graduate Program in Electrical Engineering
Federal University of Minas Gerais-Av. Antonio Carlos
6627, 31270-901, Belo Horizonte, MG, Brazil
fredericolferm@.ufmg.br, hanshs@ufmg.br

Thiago R. de Oliveira, Pedro F. Donoso-Garcia
Department of Electronic Engineering
Federal University of Minas Gerais-Av. Antonio Carlos
6627, 31270-901, Belo Horizonte, Brazil
troliveira@cpdee.ufmg.br, pedro@cpdee.ufmg.br

***Abstract*—In the present paper the modeling and control of a Dual Active Bridge (DAB) converter with input and output filters for energy storage systems (ESS) applied to DC microgrids has been described. The small-signal equivalent models are derived from the averaged circuit of the converter. Since the DAB converter with filters exhibit distinct transfer functions for charge and discharge modes, a double loop control and a method for smooth transition have been proposed. Simulations results are presented in order to evaluate the proposed control technique.**

***Keywords*—Dual Active Bridge, dc-dc converter, dc microgrid, energy storage.**

I. Introduction

Microgrids are described as small distribution power systems which employ distributed generation and power management to supply a set of local loads and that can operate connected to or isolated from the utility grid. Lately, they have become an important topic in power electronics and electrical power systems fields, since they can promote greater penetration of renewable resources (RES) to the power grid, reducing the dependency on fossil fuels, and enhance local consumer power quality, since local network dynamics can be decoupled from the utility grid. Moreover, the microgrid paradigm allows the development of local dc distribution, usually associated with residential and commercial buildings, which can substantially increase the energy efficiency of the buildings, since most loads in these environments are intrinsically dc or may operate easily from a dc bus. Therefore, dc microgrids can contribute towards net zero energy buildings.

Renewable resources have a disadvantage of being strongly dependent on climate and environmental conditions and therefore the power generation may vary considerably. Isolated microgrids based on RES may experience instability in case of a mismatch between supply and demand. In order to mitigate this problem and to smooth out energy balance, ESS in microgrids have been considered independently of utility grid connection. Due to the natural dc behavior of the accumulators, batteries and supercapacitors, a dc-dc converter must be used to interface the ESS and the microgrid dc bus.

This work has been supported by the Brazilian agency CAPES.

The energy storage converter must exhibit mainly bidirectional power flow capability and a high conversion rate depending on the voltage levels employed. Many topologies have been proposed to this sort of application with special attention to the DAB converters. A DAB converter consists of two full bridges connected to a high frequency transformer and an auxiliary inductor. Bidirectional power flow can be achieved controlling both bridges to apply phase-shifted square or quasi-square voltage waveforms across the terminals of the transformer, which depend on the modulation techniques. The most simple and traditional modulation scheme is the Phase Shift Modulation (PSM) used in [1]. More elaborated schemes have been developed to improve figures of merit such as zero voltage switching (ZVS) and conduction/switching losses across the entire operation range but at the expense of complexity [2].

Besides the minimum requirements for ESS applications, the DAB converters have advantages over other dc-dc topologies such as high power density, high power efficiency and low number of devices [3], [4], which makes this converter a very attractive candidate to interface an ESS and a microgrid dc bus. On the other hand, a relevant drawback is the high ripple content of the converter input/output currents. To suppress the injected/output current ripples into the microgrid dc bus and ESS, low pass filters are connected to both sides of a DAB converter. The circuit of the proposed converter with filters is shown in Fig. 1.

The control of the converter must take into account the bidirectional power flow according to the microgrid operating point. Since the DAB converter exhibit different transfer functions for charging and discharging modes, one current controller with adaptive parameters or two current controllers with fixed parameters must be used. In this paper two current controllers are employed. The microgrid dc bus and the ESS voltages are also controlled while discharging and charging respectively. Seamless mode transition are achieved with a finite state machine (FSM) based on [5].

This paper is organized as follows: Section II discusses the modeling of the DAB converter. Section III describes the control of the DAB converter. Section IV presents the FSM

978-1-5090-5339-1/17/$31.00 ©2017 IEEE

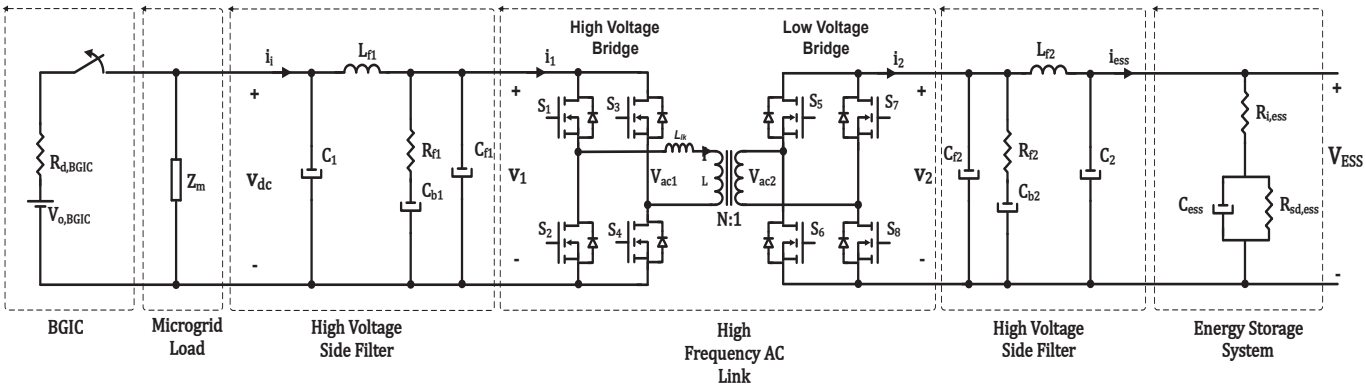

Fig. 1: DC microgrid and DAB converter with proposed filters.

used for smooth transition. Section V presents case studies. Finally, Section VI summarizes the contribution of this work.

II. Small signal model of the Dual Active Bridge

The modeling of the DAB converter has been presented in the literature using different techniques, which can be divided into simplified averaged model, continuous-time model and discrete-time model. In [3],[6],[7] the simplified averaged model is obtained from the input and output average currents, related to each other by the transformer ratio. The small signal model is extracted through conventional perturbation and linearization techniques [8]. In [9] an averaged model that considers conduction and transformer power losses is presented. In [10] the modeling and control of the DAB converter has been achieved with gyrator theory, which resembles the method employed in [3],[6],[7]. A continuous-time averaged model of the DAB converter which uses the dc and first order terms of transformer current and capacitor voltage as state variables is presented in [4]. In [17] employed state-space averaged over onde half cycle to derive the small-signal transfer functions. In [11] an accurate small-signal model discrete time for automotive DAB converter is detailed. The model yields highly accurate results at the expense of more mathematical effort. Discrete-time modeling is also discussed in [12],[13].

This paper uses the averaged model presented in [3],[7]. In this approach, the auxiliary inductor, high frequency transformer and switches are substituted by dependent current sources and the converter is represented by its terminal average currents I_1 and I_2, which are identified in Fig. 1. In fact, neglecting those devices will lead to a model lower accurate than the others. However, a simpler model facilitates the design of the controllers and may serve as the starting point for the design of the converter after defining the microgrid and ESS at system-level.

The terminal average currents can be calculated from the power flow expression for the DAB converter. Considering fixed terminal voltages V_1 and V_2, it has been demonstrated in [14] that the power transferred with PSM can be expressed as

$$P = \frac{NV_1V_2d(1-|d|)}{2L_{lk}f} \quad 0.5 \leq d \leq 0.5 \tag{1}$$

where N is the transformer voltage ratio, V_1 and V_2 are the terminal voltages of the DAB converter, L_{lk} represents the auxiliary inductor plus the transformer leakage inductance, f is the switching frequency and d is the phase shift. The literature also uses the phase shift φ, which is given in radians. The relation between d and φ is $d = \varphi/\pi$. From (1) the average terminal currents are expressed as

$$I_1 = \frac{NV_2d(1-|d|)}{2L_{lk}f} \tag{2}$$

$$I_2 = \frac{NV_1d(1-|d|)}{2L_{lk}f} \tag{3}$$

Perturbing the average currents around an operation point, we need to consider the variables as averaged values plus a small-signal such as: $v_1 = V_1 + \hat{v}_1$, $v_2 = V_2 + \hat{v}_2$ and $d = D + \hat{d}$, where the upper case letters are the dc operating points and the hatted letters are the small-signals variables. As only small-signal behavior is under evaluation, the dc terms are ignored. Assuming that the first order terms will be significantly more predominant than second order terms, the model nonlinearities can be neglected [8]. Therefore, the linearized small-signal model can be described as (4) and (5). The small-signal model equivalent circuit is shown in Fig. 2.

$$\hat{i}_1 = G_{i1d}\hat{d} + G_{i1v2}\hat{v}_2 \tag{4}$$

$$\hat{i}_2 = G_{i2d}\hat{d} + G_{i2v1}\hat{v}_1 \tag{5}$$

where

$$G_{i1d} = \left.\frac{\hat{i}_1}{\hat{d}}\right|_{\hat{v}_2=0} = \frac{NV_2(1-2|D|)}{2L_{lk}f} \tag{6}$$

$$G_{i1v2} = \left.\frac{\hat{i}_1}{\hat{v}_2}\right|_{\hat{d}=0} = \frac{ND(1-|D|)}{2L_{lk}f} \tag{7}$$

$$G_{i2d} = \left.\frac{\hat{i}_2}{\hat{d}}\right|_{\hat{v}_1=0} = \frac{NV_1(1-2|D|)}{2L_{lk}f} \tag{8}$$

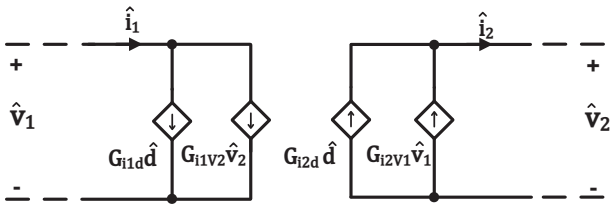

Fig. 2: Dual Active Bridge small-signal model.

Table I: Low-pass filters parameters

Parameters	Values	
	High side filter	***Low side filter***
L_f	$5\mu H$	$0.3\mu H$
C_f	$10\mu F$	$220\mu F$
C_b	$33\mu F$	$660\mu F$
R_f	0.5Ω	0.026Ω

$$G_{i2v1} = \left.\frac{\hat{i}_2}{\hat{v}_1}\right|_{\hat{d}=0} = \frac{ND(1-|D|)}{2L_{lk}f} \tag{9}$$

Since the DAB is a bidirectional converter, the direction of the power flow must be considered when using the small-signal model. According to Fig. 1 and (1)-(2), if the phase shift d is positive the power flow is from V_1 to V_2 and the small-signal model is identical to the circuit shown in Fig. 2. On the other hand, if the power flow is from V_2 to V_1, the directions of all dependent currents of the small-signal model shown in Fig. 2 are reversed, which are particularly important for transfer functions extraction.

The DAB converter input and output currents i_1 and i_2 exhibit high current ripples, which are undesirable from the point of view of the microgrid and the ESS. Thus, input/output LC low-pass filters with a RC parallel damping branches have been used to mitigate current and voltage ripples [8]. Calculations have been done to keep the maximum harmonic currents of i_1 and i_2 at twice the switching frequency equal to approximately one fourth of their nominal values. The design procedure employed is based on [14], but with a RC parallel damping branch. The filter topology is shown in Fig. 1 and the values are listed in Table I.

With the small-signal model and the filter topology we can finally derive the control-to-output transfer functions. The control to ESS current transfer functions for charging and discharging modes G^c_{iessd} and G^d_{iessd} respectively are shown in Fig. 3 and 5 respectively, whereas the control to ESS voltage transfer function for charging G^c_{vod} and the control to microgrid dc bus G^d_{vid} for discharging mode are shown in Fig. 4 and 6 respectively for $D = 0.3$. The parameters used are shown in Table III. For comparison purposes the analytical transfer functions are compared with the transfer functions extracted from the small-signal model, averaged circuit model and complete circuit, which were obtained through ac sweep with PSIM. The Bode plots show that the averaged circuit, small-signal model and the analytical expressions have approximately the same results for magnitude response. The complete

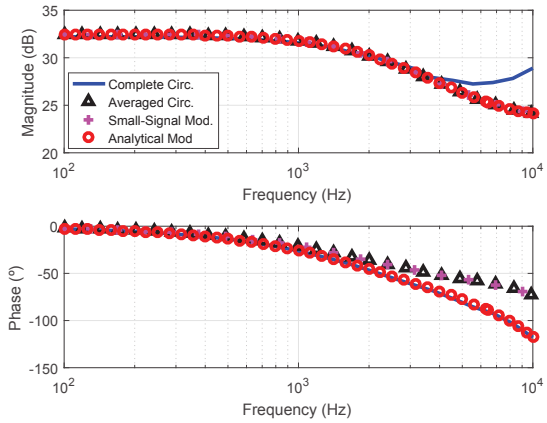

Fig. 3: Frequency response of the control to ESS current G^c_{iessd} transfer function for charging mode. Curve with "-" represent the complete model, "Δ" represent the averaged circuit,"+" represent the small-signal model and "o" represent the analytical model.

circuit presents similar magnitude response until about 4kHz, but deviates from the other after this frequency. The small-signal model phase response is identical to the averaged circuit phase response. The complete circuit exhibit significative phase deviation from the others due to the presence of the modulator and switches. In order to adequately account the phase deviation the analytical expressions must include a time delay transfer function $e^{-s\tau}$.

As shown in (6)-(9), the transfer functions derived from the small-signal model are essentially static gains, which values are highly dependent of the average phase shift D. Fig. 7 shows this dependence for $0 \leq D \leq 0.5$. The parameters used are shown in Table III. As can be seen, the gains can vary significantly according to the power flow of the converter.

III. Control of Dual Active Bridge Converter

This paper considers a DAB converter modulated with PSM to interface an ESS and a droop based microgrid dc bus. When the Bidirectional Grid Interface Converter (BGIC) and/or RES connected to the microgrid supply enough energy to charge the ESS, both current and voltage of the ESS are controlled during the process. On the other hand, if a lack of energy exists the ESS must discharge to supply the remaining power to the load connected to the microgrid dc bus. When discharging, the output current of the ESS and the dc bus are the controlled variables. Therefore, an inner current loop and an outer voltage loop for charge and discharge modes are employed, consisting of a double loop control as shown in Fig. 8. In Fig. 8 G^c_i and G^c_v are the current and voltage controllers for charging mode, respectively; G^d_i and G^d_v are current and voltage controllers for discharging mode, respectively; G^c_1 is the ESS current to ESS voltage transfer function for charging mode; G^d_1 is the ESS current to microgrid dc bus transfer function for discharging

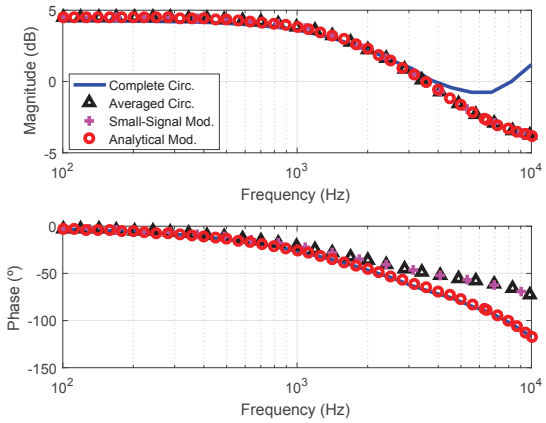

Fig. 4: Frequency response of the control to ESS voltage G^c_{vod} transfer function for charging mode. Curve with "-" represent the complete model, "Δ" represent the averaged circuit, "+" represent the small-signal model and "o" represent the analytical model.

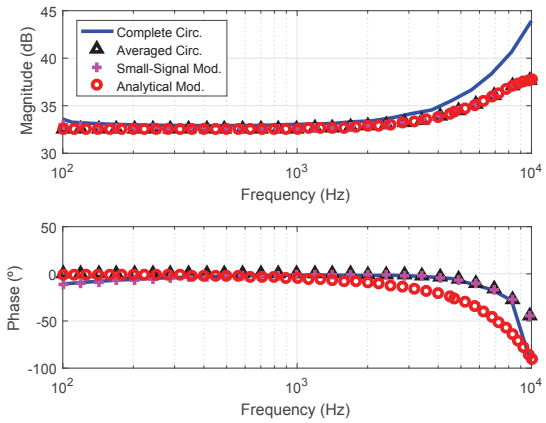

Fig. 5: Frequency response of the control to ESS current G^d_{iessd} transfer function for discharging mode. Curve with "-" represent the complete model, "Δ" represent the averaged circuit, "+" represent the small-signal model and "o" represent the analytical model.

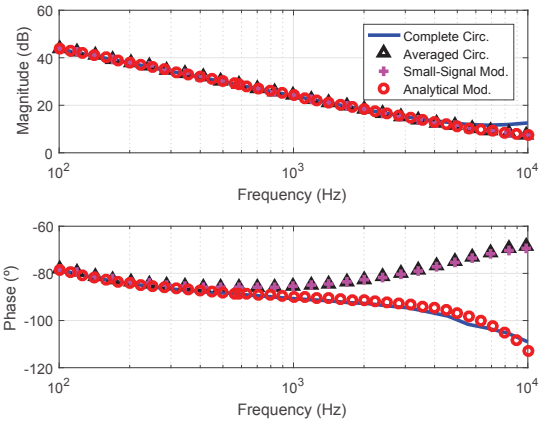

Fig. 6: Frequency response of the control to microgrid dc bus voltage G^d_{vid} transfer function for discharging mode. Curve with "-" represent the complete model, "Δ" represent the averaged circuit, "+" represent the small-signal model and "o" represent the analytical model.

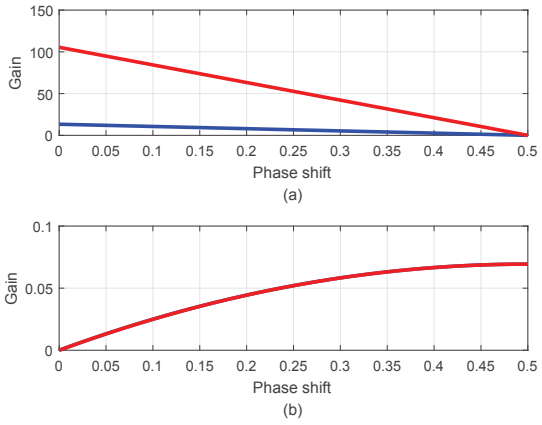

Fig. 7: Small-signal transfer functions variation with phase shift for (a) G_{i1d} in blue and G_{i2d} in red and (b) G_{i1v2} in blue and G_{i2v1} in red.

mode; G_{mod} is the modulator gain, R_d is the droop resistance of the DAB converter.

The transfer functions G^c_{iessd} and G^d_{iessd} can be calculated as (10) and (11) respectively, where Z_{Lf2}, Z_{Cf2}, Z_{Cb2} are the low side voltage filter branch impedances, Z_{C2} is the capacitor C_2 impedance and Z_{ess} is the ESS equivalent RC circuit. Since G^c_{iessd} and G^d_{iessd} are different, separate current control have been proposed. The compensated current open loop transfer functions for charging and discharging modes T^c_i and T^d_i respectively, are described as

$$T^c_i = G^c_{iessd} G_{mod} G^c_i \tag{12}$$

$$T^d_i = G^d_{iess} G_{mod} G^d_i \tag{13}$$

As the static gains of the small-signal model transfer functions vary with D, the design procedure of the current controller must take this variation into account. For both operation modes the current controllers must guarantee adequate crossover frequency and minimum phase margin across the entire operation range. In this paper PI controllers are proposed for current control and were tuned using the pole placement method with parameters shown in Table II.

The compensated voltage open loop transfer functions for charging and discharging modes T^c_v and T^d_v respectively, are described as

$$T^c_i = G^c_1 I^c_{ess,cl} G^c_v \tag{14}$$

$$T^d_i = G^d_1 I^d_{ess,cl} G^d_v \tag{15}$$

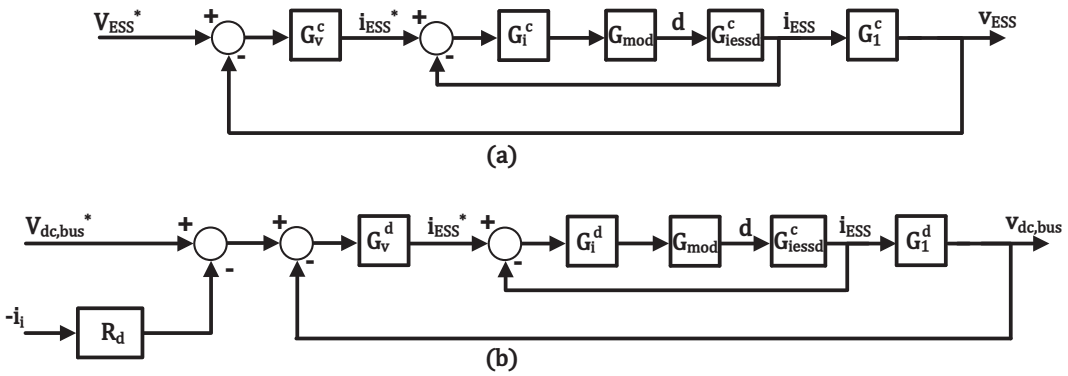

Fig. 8: Dual Acive Bridge converter control block diagram.

$$G^c_{iessd} = \left.\frac{\hat{i}_{ess}}{\hat{d}}\right|_{charge} = G_{i2d} \cdot \frac{Z_{Cf2}//Z_{Cb2}}{Z_{Cf2}//Z_{Cb2} + Z_{Lf2} + Z_{C2}//Z_{ess}} \cdot \frac{Z_{C2}}{Z_{C2} + Z_{ess}} \tag{10}$$

$$G^d_{iessd} = \left.\frac{\hat{i}_{ess}}{\hat{d}}\right|_{discharge} = G_{i2d} \cdot \frac{Z_{Cf2}//Z_{Cb2}}{Z_{Cf2}//Z_{Cb2} + Z_{Lf2}} \tag{11}$$

where $I^c_{ess,cl}$ and $I^d_{ess,cl}$ are the current closed loop transfer functions for discharging and charging mode respectively. The transfer functions G^c_1 and G^d_1 are calculated as (16) and (17) respectively, where Z_m is the microgrid load impedance, Z_{Lf1}, Z_{Cf1}, Z_{Cb1} are the high side voltage filter branch impedances, Z_{C1} is the capacitor C_1 impedance.

$$G^c_1 = Z_{ess} \tag{16}$$

As can be seen in (17) the voltage open loop transfer function in discharge mode may have its static gain varied depending on the power flow. Likewise the method described for the current loop, the voltage controllers must be tuned to ensure converter stable operation for all phase shift allowed values. The parameters of the proposed PI voltage controllers were tuned using the same procedure used for the current controllers and are shown in Table II.

The operation range of the DAB converter is limited to $0 \leq |d| \leq 0.3$, since increasing the phase shift the conduction losses are increased due to the reactive power flow in the transformer [3]. For this range and the controller gains tuned the minimum phase margin and crossover frequency range are shown in Table II for the inner current loops and outer voltage loops. As can be seen, the static gain variations of the small-signal model modify the current loops crossover frequencies. On the other hand, the voltage crossover frequencies were not modified significantly.

The major advantage of the fixed parameters is the ease to tune the gains of the PI controllers. On the other hand, it is not possible to keep the same phase margin and crossover frequency for the entire operation range, since the small-signal transfer functions modify the static gain of the forward path loop according to the phase shift value. This means that the performance of the converter will vary across the operation range. To improve performance, in [15] the proportional gain of the PI controllers used to control the DAB converter is adaptively recalculated at every sampling time. The results showed that the adaptive PI achieved consistent performance across all the operating conditions, but at the expense of more effort in controller design.

Assuming that the low-pass filters suppress sufficiently the harmonic content of the currents no filter has been considered to measure the controlled variables. In addition, for simplification purposes, sensors have been defined with unity gain and therefore provide unity feedback loop. Otherwise, the sensor gains would be inserted in the feedback loop and the forward path transfer functions would vary.

IV. Transition control

Bidirectional control with two control loops is achieved only if an adequate transition is accomplished [5]. Unfortunately most papers about DAB converter lack the power flow transition. In [16] a smooth transition between charging and discharging operation modes was achieved with the use of one current controller and two competitive voltage loops. In this paper a double loop control is employed, thus the technique used in [16] is not applicable. Therefore to switch between charge and discharge modes a FSM based on [5] has been developed. The algorithm detects the microgrid operation point using the dc bus according to the microgrid droop design and defines which control loop must be used. When a transition is detected, the algorithm enters in a special state. Neither control loops are used, but the last phase shift passed as reference to the modulator is sampled and directly increased or decreased to drive the ESS current gradually toward zero. The current rate can be easily adjusted through a designer defined phase shift step value. When the current is near zero and dc bus voltage conditions are satisfied, charging or discharging mode is set and the loop switching is effectively accomplished. To avoid instabilities, voltage and current hysteresis have been

$$G_1^d = Z_m \cdot \frac{Z_{C1}}{Z_{C1} + Z_m} \cdot \frac{Z_{Cf1}//Z_{Cb1}}{Z_{Cf1}//Z_{Cb1} + Z_{Lf1} + Z_{C1}//Z_m} \cdot \frac{G_{i1d}}{G_{i2d}} \frac{Z_{Cf2}//Z_{Cb2} + Z_{Lf2}}{Z_{Cf2}//Z_{Cb2}} \tag{17}$$

Table II: Controller parameters

Mode	Loop	Controller gains	Phase margin	Crossover frequency
Charge	Current	$K_p = 0.0038$ $K_i = 180.95$	$PM > 57°$	$1.1 - 2.3kHz$
	Voltage	$K_i = 300$	$PM > 76.9°$	$1.95Hz$
Discharge	Current	$K_i = 284.59$	$PM > 57°$	$1.95 - 7.7kHz$
	Voltage	$K_p = 0.43$ $K_i = 338.02$	$PM > 76.9°$	$195.7Hz$

Table III: Parameters used in simulation

Symbol	Parameters	
	Description	***Value***
V_1	High side nominal voltage	380V
V_2	Low side nominal voltage	48V
N	Transformer ratio	7.94
L_{lk}	Auxiliary inductance plus transformer leakge inductance	715.42 μH
f	Switching frequency	20kHz
$P_{nom,DAD}$	DAB nominal power	1kW
R_d	DAB droop resistance	3.6Ω
$P_{nom,BGIC}$	BGIC nominal power	3kW
V_{BGIC}	BGIC open circuit voltage	380V
$R_{d,BGIC}$	BGIC droop resistance	1.23Ω
Z_m	Microgrid load	$R = 144.4\Omega$ $C = 1000\mu F$
$R_{i,ess}$	ESS internal resistance	$40m\Omega$
$R_{sd,ess}$	ESS self-discharge resistance	490.34Ω
C_{ess}	ESS stored charge capacitance	$8.75F$
G_{mod}	Phase Shift Modulator gain	1

used for mode detections. Simulations results are carried out to verify the proposed smooth transition control.

V. Simulation Results

The circuit used for simulation is shown in Fig. 1. The ESS was modeled as simplified RC circuit where $R_{i,ess}$ is the ESS internal resistance, $R_{sd,ess}$ is the resistance for self-discharge current and C_{ess} is to represent stored charge with 105Ah of capacity. The BGIC used to connect the microgrid dc bus to the utility grid is modeled as a voltage source V_{BGIC} in series with its droop resistance $R_{d,BGIC}$. The parameters used in simulation are shown in Table III.

Fig. 9 shows the ESS current for charging to discharging and discharging to charging transition. Until 50ms, the DAB converter is operating in charging mode with nominal charge current (11A). At t=50ms, the BGIC is disconnected from the microgrid. The control algorithm detects a charging-discharging transition and the phase shift is linearly decreased to lead ESS current to zero as depicted in Fig. 10a and 11a. When the current is sufficiently small (1A), discharge mode

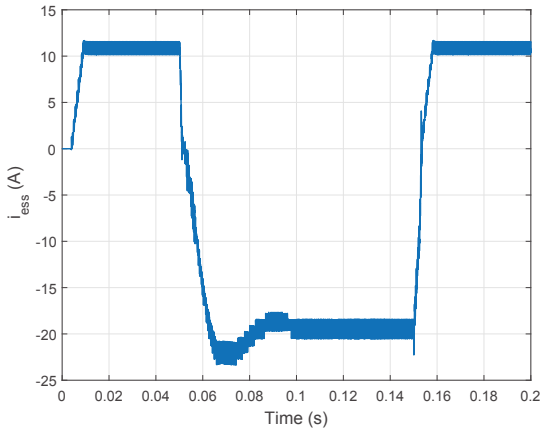

Fig. 9: Energy Storage System current i_{ess} in (a) charging to discharging transition and (b) discharging to charging transition.

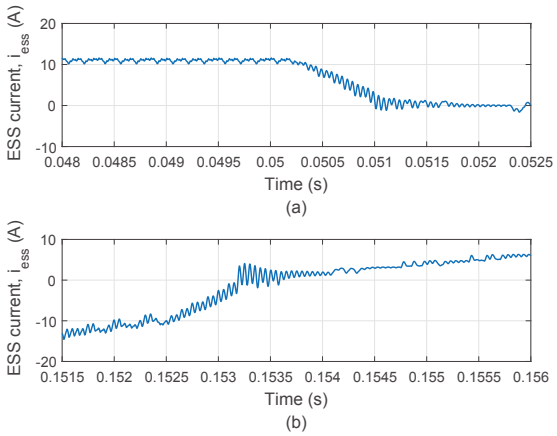

Fig. 10: Detailed Energy Storage System current i_{ess} during transition mode.

is set and ESS current grows negatively down to the nominal discharge value (-22A) to supply the dc bus voltage according to the droop characteristic. At t=150ms, the switch is closed. The algorithm detects a discharge-charge transition and drives the phase shift to increase ESS current toward zero, as shown Fig. 10b and 11b. When the current approaches -1A, charge mode is set and the ESS current rises until the nominal charge current (11A).

The dc bus voltage is shown in Fig. 12. During charge-discharge transition the voltage drops due to the microgrid load and the ESS discharges to control de microgrid dc bus voltage. At t=150ms the BGIC is reconnected and resumes the microgrid dc bus voltage control. Thus, the ESS can operate again in charging mode. In order to mitigate the dc bus voltage

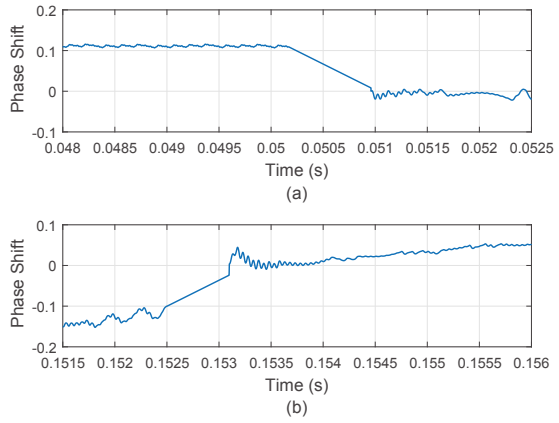

Fig. 11: Phase shift reference in (a) charging to discharging transition and (b) discharging to charging transition with dd/dt=127.7/s.

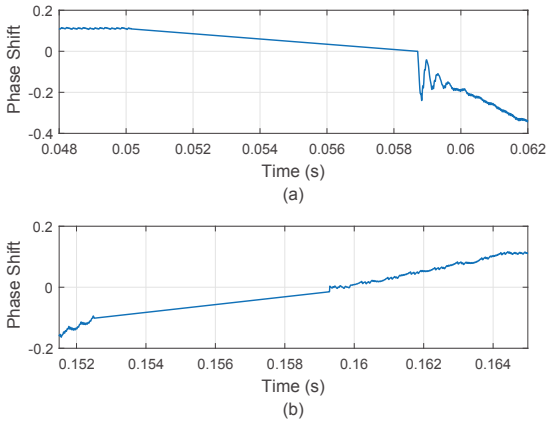

Fig. 13: Phase shift reference in (a) charging-to-discharging transition and (b) discharging to charging transition with dd/dt=12.77/s.

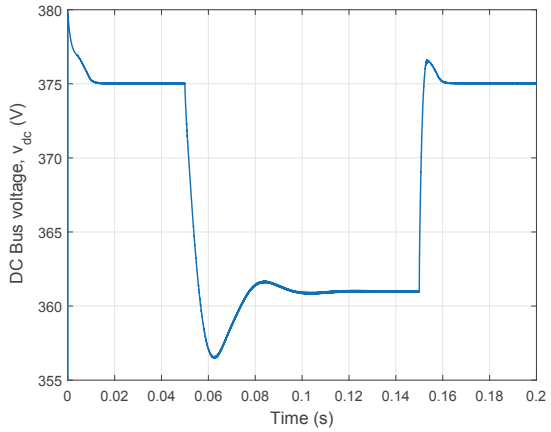

Fig. 12: DC Bus voltage for charging to discharging and discharging to charging transition.

drop during charging to discharging transitions, the capacitor C_1 can be increased.

Fig. 11 and 13 show ESS current for the same microgrid operation conditions but with derivatives of phase shift (dd/dt) of 127.7/s and 12.77/s respectively. At t=50ms the FSM detected a charge-discharge transition. The last phase shift passed by the charging loop is sampled and is used as reference for the DAB converter. The phase shift is reduced step by step until the ESS approximates zero. With dd/dt=12.77/s 8.6ms were necessary to lead to ESS current to zero, whereas with dd/dt=127.7/s approximately 1.0ms passed. Therefore, higher phase shift derivatives lead the ESS current to zero faster. The phase shift derivative is easily adjusted by software and can be used to control the rate ESS current during transition mode.

VI. Conclusion

In this paper the modeling and control of a DAB converter with input/output filters is presented. The small-signal model derived from the averaged DAB converter was employed to state the transfer functions necessary for controlling the converter. Bode plots indicated that the control-to-output transfer functions analytically derived are in accordance with the ones extracted from simulation models. PI controllers with fixed parameters are proposed for the double loop control employed.

A FSM is proposed to control the DAB converter operation modes. When a transition is detected the FSM drives the phase shift applied to the modulator adequately to achieve smooth transition. The rate of the ESS current during transitions can be easily adjusted by software.

Acknowledgment

This work has been supported by the Brazilian agency CAPES.

References

[1] R. W. A. A. De Doncker, D. M. Divan and M. H. Kheraluwala, "A three-phase soft-switched high-power-density DC/DC converter for high-power applications," in *IEEE Transactions on Industry Applications*, vol. 27, no. 1, pp. 63-73, Jan/Feb 1991.

[2] Y. A. Harrye, K. H. Ahmed, G. P. Adam and A. A. Aboushady, "Comprehensive steady state analysis of bidirectional dual active bridge DC/DC converter using triple phase shift control," *2014 IEEE 23rd International Symposium on Industrial Electronics (ISIE)*, Istanbul, 2014, pp. 437-442.

[3] A. Rodriguez Alonso, J. Sebastian, D. G. Lamar, M. M. Hernando and A. Vazquez, "An overall study of a Dual Active Bridge for bidirectional DC/DC conversion," *2010 IEEE Energy Conversion Congress and Exposition*, Atlanta, GA, 2010, pp. 1129-1135.

[4] H. Qin and J. W. Kimball, "Generalized Average Modeling of Dual Active Bridge DCDC Converter," in *IEEE Transactions on Power Electronics*, vol. 27, no. 4, pp. 2078-2084, April 2012.

[5] Saichand, K; Vinod, John. Virtual resistance based control for Ultracapacitor based Bidirectional dc-dc Backup System. Department of Electrical Engineering Indian Institute of Science, Bengaluru, 2015.

[6] H. K. Krishnamurthy and R. Ayyanar, "Building Block Converter Module for Universal (AC-DC, DC-AC, DC-DC) Fully Modular Power Conversion Architecture," *2007 IEEE Power Electronics Specialists Conference*, Orlando, FL, 2007, pp. 483-489.

[7] Guacaneme, J., Garcer, G., Figueres, E., Patrao, I., and Gonzlez-Medina, R. (2015) Dynamic modeling of a dual active bridge DC to DC converter with average current control and load-current feed-forward. Int. J. Circ. Theor. Appl., 43: 13111332.

[8] Erickson, R. W.; Maksimovic, D. Fundamentals of Power Electronics. 2ed. Springer, 2001.

[9] K. Zhang, Z. Shan and J. Jatskevich, "Large- and Small-Signal Average-Value Modeling of Dual-Active-Bridge DCDC Converter Considering Power Losses," in *IEEE Transactions on Power Electronics*, vol. 32, no. 3, pp. 1964-1974, March 2017

[10] Martins, W. M. D. S. e D. C. Modelagem e controle dos conversores dab e tab utilizando a teoria do gyrator. In: *XIX Congresso Brasileiro de Automatica*. [S.l.: s.n.], 2012.

[11] F. Krismer and J. W. Kolar, "Accurate small-signal model for an automotive bidirectional Dual Active Bridge converter," *2008 11th Workshop on Control and Modeling for Power Electronics*, Zurich, 2008, pp. 1-10.

[12] Ling Shi, Wanjun Lei, Jun Huang, Zhuoqiang Li, Yao Cui and Yue Wang, "Full discrete-time modeling and stability analysis of the digital controlled dual active bridge converter," *2016 IEEE 8th International Power Electronics and Motion Control Conference (IPEMC-ECCE Asia)*, Hefei, 2016, pp. 3813-3817.

[13] D. Costinett, R. Zane and D. Maksimovi, "Discrete-time small-signal modeling of a 1 MHz efficiency-optimized dual active bridge converter with varying load," *2012 IEEE 13th Workshop on Control and Modeling for Power Electronics (COMPEL)*, Kyoto, 2012, pp. 1-7.

[14] Krismer, F. Modeling and optimization of bidirectional dual active bridge DC-DC converter topologies. Thesis, Swiss Federal Institute of Technology, 2010.

[15] Segaran, Dinesh Sekhar. Dynamic Modelling and Control of Dual Active Bridge Bi-Directional DC-DC Converters for Smart Grid Applications. Thesis, Royal Melbourne Institute of Technology University, 2006.

[16] W. W. A. G. Silva, P. F. Donoso-Garcia, S. I. Seleme, T. R. Oliveira, C. H. G. Santos and A. S. Bolzon, "Study of the application of bidirectional dual active bridge converters in dc nanogrid energy storage systems," *2013 Brazilian Power Electronics Conference*, Gramado, 2013, pp. 609-614.

[17] G. D. Demetriades and H. P. Nee, "Dynamic modeling of the Dual-Active Bridge topology for high-power applications," 2008 IEEE Power Electronics Specialists Conference, Rhodes, 2008, pp. 457-464.